Search for cluster states with negative parities above double shell closures

Tao Wan and Yibin Qian*
Department of Applied Physics and MIIT Key Laboratory of Semiconductor Microstructure and Quantum Sensing, Nanjing University of Science and Technology, Nanjing 210094, China

Hankui Wang†
Department of Physics and Key Laboratory of Optical Field Manipulation of Zhejiang Province, Zhejiang Sci-Tech University, Hangzhou 310018, China

(Received 19 December 2023; revised 5 June 2024; accepted 8 July 2024; published 19 July 2024)

The persistence of α-cluster states in light nuclei has aroused great interest in nuclear physics during the past several decades, and the cluster-core configuration is expected to play a key role in interpreting the spectroscopic properties of heavier nuclei. In this study, we have systematically investigated the energy spectra of α-cluster structures above the double shell closures within the binary cluster-core model (BCM), especially for rotational bands with negative parities. The reliability and integrity of BCM can be proved by the excellent reproduction of energy spectra. Analogously, this kind of picture is generalized to the case of heavier clusters above doubly magic core ^{208}Pb by modifying the quantum condition for the number of nodes in the cluster-core wave function. The uncertainties of relevant parameters in the nuclear potential are determined by the nonparametric resampling strategy, leading to our statistical results on these states with negative parities. It is hoped that our present study can stimulate further insight into clustering phenomena of heavy and superheavy nuclei.

DOI: 10.1103/PhysRevC.110.014318

I. INTRODUCTION

Clustering is a fundamental dynamical feature [1] of microscopic many-body physics that exists in various composite systems, such as the clusters of micro-organisms or the binding of atoms within the molecules. When it comes to the atomic nucleus, the clustering structure as one cornerstone of nuclear systems has shed new light on the basic unit of nuclei. As early as 1937, Wheeler [2] introduced the concept of clusters into the description of nuclear relative motion. In this picture, the nucleon clustering occurs in a delicate balance among Coulomb repulsion, Pauli blocking effect, and nuclear force. α cluster with two valence neutrons and two valence protons is the essential subunit within a nucleus to investigate properties of $n\alpha$ nuclei or the systems of $n\alpha$ plus other particles [3] due to the quite large binding energy per nucleon and high first excitation energy. From this perspective, the α cluster was used in an intuitive way to interpret some interesting phenomena about binding energy [4]. However, this interpretation is quite rough, in particular when more microscopic ingredients should be considered, such as the configuration interaction. Less attention was paid to the clustering in light nuclei until the improvement of experimental facilities and the proposal of the Ikeda diagram [5]. There has been much progress [1,6–9] the experimental observations, especially for the α-conjugate nuclei, which strongly increased interest in further understanding of cluster configurations. For example, some exotic cluster states in light nuclei have been observed very recently, such as the condensatelike $\alpha + {}^2n + {}^2n$ structure in ^{8}He [10] and 4α structure in ^{16}O [8].

In addition to the experimental progress mentioned above, various microscopic cluster models [11] have been proposed to demonstrate the reliability of α-cluster configurations, such as the generator coordinate method (GCM), the resonating group method (RGM), and the orthogonality condition model (OCM). Other sophisticated cluster models and approaches have been developed for the calculations of cluster states, such as the quantum Monte Carlo (QMC) method [12], the fermionic molecular dynamics (FMD) [13,14], the antisymmetrized molecular dynamics (AMD) [15–17], and the Tohsaki-Horiuchi-Schuck-Röpke (THSR) wave function [18–22] plus the extension to the picture of nonlocalized clustering. Despite the evidence of the existence of α clusters throughout the light mass region, the generation of α clusters in heavier nuclei appears to be more ambiguous due to the complicated interaction among nucleons with the increase of mass number. On the other hand, the α-like correlations in heavy nuclei may be suppressed by larger spin-orbit force, which leads to a dilemma of cluster structures in the increasing competition with mean-field structure. Hence, a natural but challenging question is whether there exists α-cluster or other clustering phenomenon when it comes to heavier nuclei. For instance, One widely accepted consensus is that the α cluster is believed to exist at the surface of the mother nucleus in the α-decay process [23]. Subsequently, α clusters and daughter nuclei combine to construct the so-called

*Contact author: qyibin@njust.edu.cn
†Contact author: whk2007@163.com

quasibound states, which contribute to a certain decay width corresponding to experimentally observable decay events. The superallowed α decay to doubly magic ^{100}Sn was observed experimentally via the α-decay chain $^{108}\mathrm{Xe} \rightarrow {}^{104}\mathrm{Te} \rightarrow {}^{100}\mathrm{Sn}$ [24]. The formation of α clusters was first "seen" in the medium mass nuclei from the proton-induced quasifree α-cluster knockout reactions [25]. Accordingly, α decay is a possible scenario in which the α-cluster degree plays an important role. If one assumes such an "α + core" system inspired by α decay, the α-cluster states and the corresponding energy spectra plus the electromagnetic transitions should be also open to exploration. Indeed, a series of typical nuclei above doubly closed shells, that is ^{20}Ne, ^{44,52}Ti, ^{94}Mo, and ^{212}Po [23,26–40], have been regarded as a natural laboratory for investigating the rotational bands and $B(E2)$ values. In our previous work [41], the binary cluster-core model (BCM) was combined with the Monte Carlo bootstrap method to systematically study this kind of cluster structure accompanied with uncertainty evaluation.

In this study, the main aim is to give the satisfactory calculations of negative-parity rotational bands to verify the reliability of BCM. In the meantime, the description of specific process of the bootstrap method in the previous work [41] was a little vague. More details of the nonparametric resampling strategy will be presented therefore in this article. Another new point is that, such cluster states with negative parities will be extended to possible heavier cluster cases as well to further check or confirm the role of cluster degree played in the structural knowledge of heavy nuclei. This article is organized in the following way. In Sec. II, the Monte Carlo bootstrap method and calculations of energy spectra within the cluster-core model are given. We will simultaneously present the numerical results of the rotational bands of α-cluster configurations above doubly magic core and possible clusters in heavy or superheavy nuclei in Sec. III. A summary is given in the last section.

II. THEORETICAL FRAMEWORK

Besides the various aforementioned microscopic models, a simple but very effective model is the BCM. In the framework of BCM, the cluster-core relative motion, generating the cluster states, is treated as the dominant factor to describe the rotational bands of target nuclei. To achieve this, one should directly solve the two-body Schrödinger wave equation,

$$\left[\frac{-\hbar^2}{2\mu}\nabla^2 + V(r)\right]|n,l\rangle = E_{nl}|n,l\rangle, \tag{1}$$

where n, l are the principal and orbital quantum numbers respectively. Here μ is the two-body reduced mass, and $V(r)$ is the total interaction potential, which is the sum of the attractive nuclear part, repulsive Coulomb part, and centrifugal term respectively, as follows:

$$V(r) = V_N(r) + V_C(r) + \frac{\hbar^2\ell(\ell+1)}{2\mu r^2}. \tag{2}$$

The Coulomb potential $V_C(r)$ is considered as the interaction potential of the uniformly charged core with radius R_C and the daughter nucleus. In treatment of the nuclear potential $V_N(r)$, the semimicroscopic double folding potential [42–44] based on the effective nucleon-nucleon interaction has been widely applied in the calculations of rotational bands and elastic scattering cross sections. However, the ground-state rotational bands from the double folding potential have a more compressed feature compared with available data. Another good choice is the nuclear potential of phenomenological form with free parameters, which has been successful in reproducing the energy levels with positive parities of the set {^{20}Ne, ^{44}Ti, ^{94}Mo, and ^{212}Po} in our previous studies [41]. To make the study consistent, we therefore adopt the same nuclear potential of (1 + Gaussian)(W.S. + W.S.^{3}), shape [41,45,46], namely

$$V_N(r) = -V_0\left[1+\lambda\exp\left(-\frac{r^2}{\sigma^2}\right)\right] \times\left\{\frac{b}{1+\exp[(r-R)/a]}+\frac{1-b}{\{1+\exp[(r-R)/3a]\}^3}\right\}, \tag{3}$$

where the parameters λ and σ, the depth V_0, the diffuseness a, and the mixing parameter b are to be determined via the following procedure. The nuclear radii R of nuclei above the doubly magic core are then determined by reproducing the experimental 5^- member [47] of the possible α-cluster states for each nucleus during the whole calculation of the present study. In order to minimize the number of free model parameters and facilitate calculation, the radius R is assumed to be equal to the Coulomb radius R_C.

On the basis of existing models and theories, it is believed that α clusters only exist at the surface of nuclei with a low nuclear density. In other word, the valence nucleons of clusters have to occupy a higher energy level to ensure the formation of clusters, which are limited by the Wildermuth condition [48]

$$G = 2n + l = \sum_i \left(g_i^{A_d+A_c} - g_i^{A_c}\right). \tag{4}$$

Here $g_i^{A_d+A_c}$ are the oscillator quantum numbers, whose values are supposed to ensure every nucleon constituting clusters occupies higher orbits outside the frozen core. The interior quantum numbers $g_i^{A_c}$ can adjust the orbits of the nucleons inside clusters in order to better fit the Pauli exclusion principle. The global quantum number G identifying the states of bands can be obtained when $g_i^{A_d+A_c}$ and $g_i^{A_c}$ are fixed. The internal nodes n, just the principal quantum numbers, are subsequently given by the orbital angular momentum l. Hence, the restriction $G \geqslant G_{\mathrm{g.s.}}$ is taken into consideration in the negative-parity rotational bands, where $G_{\mathrm{g.s.}}$ is associated with the ground state band. The numbers $G = 9$, $G = 13$, and $G = 15$ are respectively employed for the rotational bands of the nuclei ^{20}Ne, ^{44}Ti, and ^{92}Zr in accordance with the Wildermuth condition. The value of G for the nuclei ^{94}Mo, ^{96}Ru, and ^{98}Pd can be confidently chosen as $G = 17$. In this way, the picture has been employed also in other good approximations and surface properties of the core ^{208}Pb plus larger cluster sizes, such as the isotopes of carbon and beryllium. More details will be discussed in the following section.

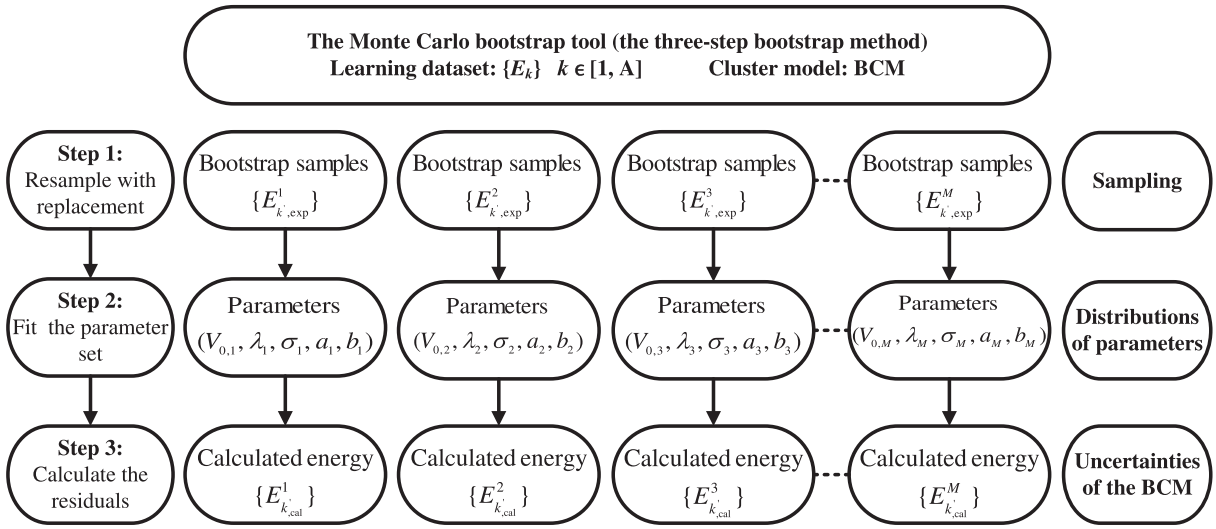

FIG. 1. A flowchart of the three-step bootstrap method.

As mentioned before, the interaction potential between the frozen core and cluster is the crucial part of such a binary cluster-core model, and is restricted by radius parameter R and other model parameters. Owing to the deficiency of available measured data for negative-parity levels of the above nuclei, the extrapolation beyond regions reached by measuring can be useful for forthcoming experimental designs or theoretical analyses. It is of great importance in this article to implement a further investigation into the determination of the propagated uncertainties from corresponding model parameters to calculated results. With the progress of modern computers, the data can be graphically presented in ways previously unimaginable. Accordingly, the test analysis of uncertainties from the perspective of statistics has recently drawn great attention in almost all research fields. When focusing on nuclear physics, some pioneering works have been carried out with statistical methods to estimate the theoretical uncertainties, like the estimation of existing α-decay formulas [49], the propagation of uncertainties in the framework of the Skyrme energy-density-functional (EDF) approach [50], and the liquid drop (LD) model [51]. In addition to traditional statistical methods such as Bayesian inference and sensitivity analysis [50,52,53], the Monte Carlo bootstrap [54] method can give more satisfactory responses by nonparametrically resampling target data without any prior assumptions and sample size limitations. One can effectively records the uncertainty information by the performance of significance tests and the calculation of confidence intervals and standard errors with the bootstrap method.

Admittedly, the key technology of the bootstrap method is resampling, which can reconstruct the distributions of parameters via the fitting procedure to quantify the uncertainty. The specific fitting procedure is presented in Fig. 1:

Step 1. Resample with replacement. Considering both the narrow error bars of energy spectra and smooth progression of the calculation procedure, these available data [55] are identified as the exact values in the process of bootstrapping without the uncertainties. So far, the α-cluster structures have been well established for ground-state $K^\pi = 0^+$ bands in the aforementioned nuclei with doubly magic core plus α particle. In contrast, the experimental information for α-cluster properties of negative-parity bands is not so clear except for ^{20}Ne with 1^- bandhead placed at 5.79 MeV [56,57] and ^{44}Ti with 6.22 MeV [31,57–59] for 1^- bandhead. Analogously to the previous investigations [34,35], the relatively complete rotational bands with negative parities for ^{94}Mo and ^{96}Ru are selected as the possible candidates for α-cluster states. The available rotational bands with negative parities, from 1^- to 9^- for ^{20}Ne, from 1^- to 7^- for ^{44}Ti, from 5^- to 13^- for ^{94}Mo, and from 5^- to 17^- for ^{96}Ru, are therefore selected as A pieces of samples, namely the original learning dataset $\{E_k\}$, where E_k is the kth sample of energy level. Resampling with replacement means that one can randomly extract a sample from the $\{E_k\}$ and then put it back before the next sampling. The new energy array called bootstrap sample $\{E^i_{k',\mathrm{exp}}\}$ can be then created by the ith resampling. It is to be noted that each bootstrap sample should be same size as the learning dataset $\{E_k\}$. In practice, the distributions of corresponding parameters can be very well approximated with sufficient replications. Thus, the replications of the process of resampling will reach M ($\approx 10^3$) times by using the computational facility. There is little additional variation occurring in the resampling process. Instead, almost all the variations of the parameter distributions originate from the selection of the random samples in the original population.

Step 2. Fit the parameter set. The key part of BCM, as mentioned before, is the cluster-core potential. The uncertainty information of BCM is derived from the uncertainty of model parameters in Eq. (3). The resample statistics of each bootstrap sample $\{E^i_{k',\mathrm{exp}}\}$ should be separately fitted to get the distributions of parameters. To be more precise, the optimal parameter set of $\{E^i_{k',\mathrm{exp}}\}$ is determined by minimizing the square deviation between the experimental rotational bands and the calculated energy levels [60], namely

$$\chi^2_i = \frac{\sum_{i=1}^{A} \left(E^i_{k',\mathrm{cal}} - E^i_{k',\mathrm{exp}}\right)^2}{A}. \tag{5}$$

With the fitting procedure, one can get dependable distributions of parameter space from the fixed M groups of optimal parameter sets, which are stored for the next bootstrap step.

Step 3. Calculate the residuals. Following this, the energy array $\{E^i_{k',\mathrm{cal}}\}$ and theoretical uncertainties of model parameters related to the cluster-core potential can be obtained simultaneously with the help of the optimal parameter sets. Furthermore, one can well reproduce the rotational bands and predict the unknown negative-parity states.

In view of uncertainty analysis with the bootstrap method, the total model uncertainties under some certain circumstances are random variables, which can be divided into three parts, including the systematic, statistical, and experimental uncertainty. The systematic uncertainty, coming from the deficiency of BCM, is expressed in the following form:

$$\hat{\sigma}^2_{\mathrm{stat},k} = \left(\bar{E}_{k,\mathrm{cal}} - E^i_{k,\mathrm{exp}}\right)^2. \tag{6}$$

Here the $\bar{E}_{k,\mathrm{cal}}$ is the average value of all calculated results of the kth energy bands, namely $\bar{E}_{k,\mathrm{cal}} = \frac{1}{M}\sum_{i=1}^{M} E^i_{k,\mathrm{cal}}$. Furthermore, the statistical uncertainty, originating from some parameters to be determined, is given by

$$\hat{\sigma}^2_{\mathrm{stat},k} = \frac{1}{M-1}\sum_{i=1}^{M}\left(E^i_{k,\mathrm{cal}} - \bar{E}_{k,\mathrm{cal}}\right)^2. \tag{7}$$

The model uncertainty of the kth energy level is determined by

$$\hat{\sigma}^2_{\mathrm{total},k} = \hat{\sigma}^2_{\mathrm{stat},k} + \hat{\sigma}^2_{\mathrm{stat},k}. \tag{8}$$

Noticeably, the experimental uncertainty based on the exact dataset $\{E_k\}$ is negligible in bootstrapping procedure for convenience. As a result, the total uncertainty is evaluated in the following form:

$$\hat{\sigma}^2_{\mathrm{total}} = \frac{1}{A}\sum_{k=1}^{A}\hat{\sigma}^2_{\mathrm{total},k} = \frac{1}{A}\sum_{k=1}^{A}\left(\hat{\sigma}^2_{\mathrm{stat},k} + \hat{\sigma}^2_{\mathrm{stat},k}\right). \tag{9}$$

According to our previous study [41] and the appropriate attempts, the two parameters a and σ are fixed as 0.500 fm and 0.342 fm, which are comparable with other studies [35,40,45,47,61]. The other three parameters V_0, b, and λ are then adjusted with the bootstrap strategy. The distributions of parameters are smoothly obtained from the M groups of optimal parameter sets in step 2. In order to better comprehend the relationship of the uncertainties and parameters, the relative frequency charts of V_0, b, and λ are presented in Fig. 2. It is clearly seen in Fig. 2 that all the distributions in the parameter space have a distinct peak, which leads to the good convergence of the parameters and high stability of the BCM. The error ranges of all parameters in the cluster-core potential are considered by calculating their mean values and standard deviations. The residual model parameters for nuclei ^{20}Ne, ^{44}Ti, ^{94}Mo, and ^{96}Ru are obtained as $V_0 = 240.677 \pm 6.244$ MeV, $b = 0.205 \pm 0.014$, and $\lambda = 0.133 \pm 0.053$, which can produce a shape of nuclear potential similar to that in other investigations [35,40,45,47,61]. With the obtained model parameter set, a comparison of the present nuclear term with (1 + Gaussian)(W.S. + W.S.^{3}) shape with the conventional W.S. potential in Ref [62] for ^{20}Ne and ^{94}Mo is shown in Fig. 3.

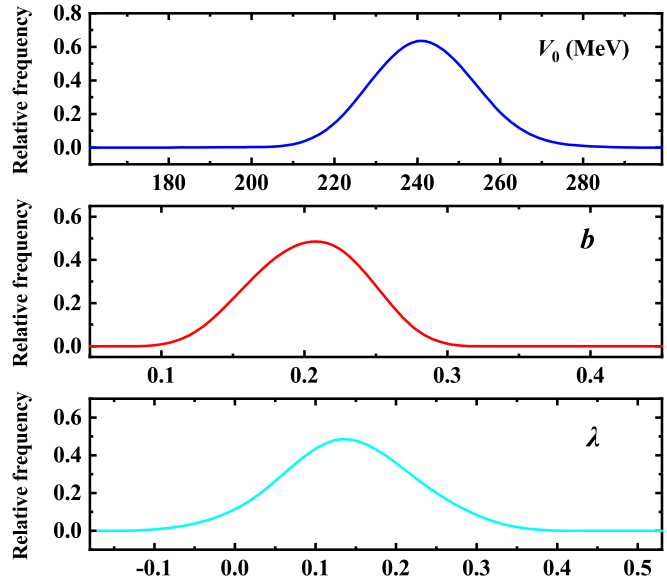

FIG. 2. Distributions of model parameters V_0, b, and λ in the nuclear potential.

The internal potential well with W.S.^{3} term [30,34,47,63] is deeper and steeper, compensating for the typical shortcoming of the inverse energy levels derived from the W.S. potential. Moreover, using the nuclear potential plus the Gaussian factor [41,45,46] can avoid the compressed bands coming from the double-folding potentials, especially for the lowest level spacing.

III. NUMEROUS RESULTS AND DISCUSSION

Through the Monte Carlo bootstrap method, we have systematically discussed the propagation of the uncertainty and the predictive ability of a cluster-core model. The complete rotational bands along with error analysis for a series of typical nuclei can be obtained thereby. In fact, identifying α-cluster structures with negative parities above double closed shells

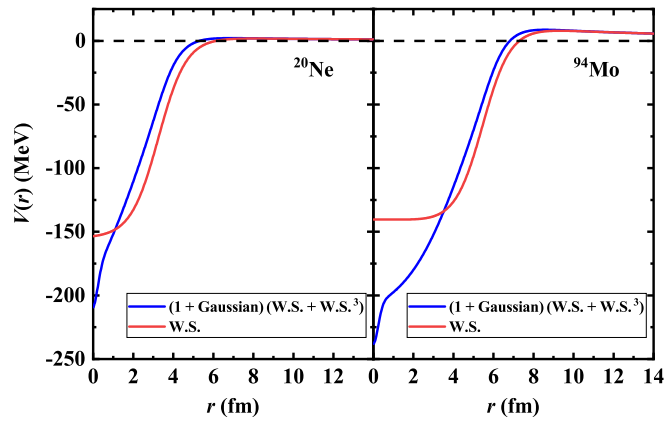

FIG. 3. Comparison between the phenomenological core-cluster interaction of (1 + Gaussian)(W.S. + W.S.^{3}) shape (blue line) in this work with the W.S. potential (red line) in Ref. [62] for ^{20}Ne and ^{94}Mo.

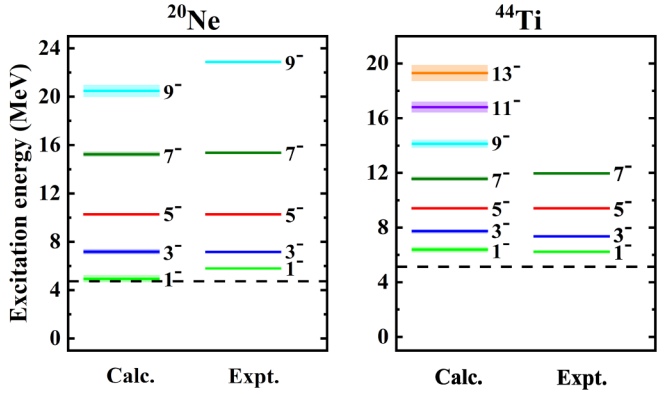

FIG. 4. The rotational bands with negative parities of ^{20}Ne ($G = 9$) and ^{44}Ti ($G = 13$), in which the shaded range indicates the uncertainty bar of theoretical energy level. The dotted lines denote the α + core breakup thresholds.

is more difficult due to the scarce experimental information. Fortunately, α-cluster configurations of $K^\pi = 0^-$ rotational bands for ^{20}Ne with 1^- bandhead lying at 5.79 MeV [56,57] and ^{44}Ti with 6.22 MeV [31,57–59] of the $J^\pi = 1^-$ state have been well established via α-transfer experiments like the (^{6}Li, d) reaction. The existence of α-cluster structures with negative parities in ^{94}Mo have been discussed in previous studies [34,35,38,39,57], and indicated that 1^- state should lie at about 7 MeV. However, the energy levels of α-cluster states fare not specific for medium mass nuclei due to the lack of complementary measured data. In the present study, the lowest $K^\pi = 0^-$ bands are regarded as the candidates of α + core rotational energy levels for ^{94}Mo and ^{96}Ru, as in Refs. [34,35]. The available experimental levels for the above four nuclei are therefore selected as the original learning dataset $\{E_k\}$ in step 1. The comparisons of calculated energy levels with the available data for ^{20}Ne, ^{44}Ti, and ^{94}Mo, ^{96}Ru are initially plotted in Figs. 4 and 5, where the α + core breakup thresholds are indicated by the dotted lines. The uncertainty bars, corresponding to the shaded ranges, are determined by one standard deviation around the mean values of theoretical energies. It is found that the range of the uncertainty bar is gradually increasing further away from the 5^- state, and all errors are relatively

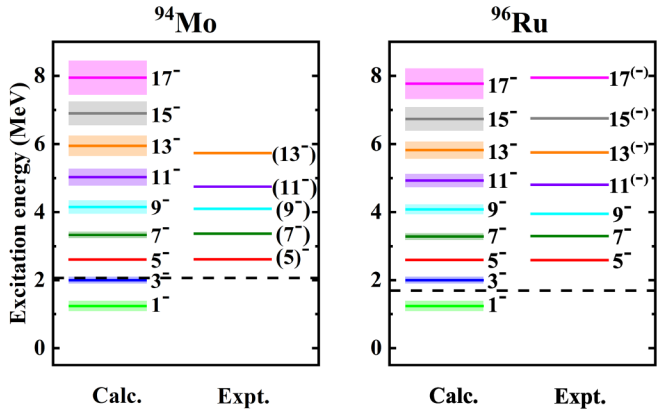

FIG. 5. Same as Fig. 4 but for ^{94}Mo ($G = 17$) and ^{96}Ru ($G = 17$).

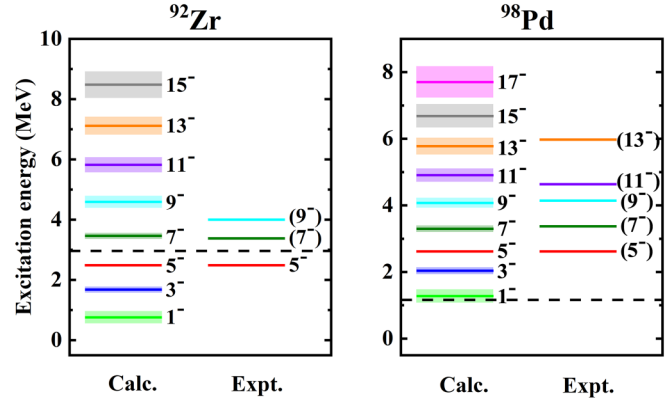

FIG. 6. Same as Fig. 4 but for ^{92}Zr ($G = 15$) and ^{98}Pd ($G = 17$).

small. The calculated results for $K^\pi = 0^-$ negative-parity bands are in good agreement with the experimental spectra expect for the 9^- state of ^{20}Ne. As shown in Figs. 4 and 5, the available data for ^{44}Ti, ^{94}Mo, and ^{96}Ru are insufficient concerning $K^\pi = 0^-$ bands. It would be worthwhile to provide the predictions on complete theoretical negative-parity bands within the BCM not only for experimental design, but also for theoretical analysis. The good agreement of our results with energy spectra plus the narrow uncertainty bars prove that the binary cluster-core model is useful for describing the possible α-cluster structures in light and medium mass nuclei with the help of suitable statistic analysis. In order to further verify the reliability of the BCM, the present process with the same parameter set in Eq. (3) was subsequently applied into other α + core nuclei near the nucleus ^{94}Mo, namely ^{92}Zr and ^{98}Pd. The obtained results are compared with the corresponding energy levels in Fig. 6, where one can also get satisfactorily theoretical spectra plus narrow uncertainty bars. All the results denote that such a binary cluster-core model introduces small errors in calculations and exhibits reasonable global predictive capability, which is beneficial to investigate the negative-parity bands in heavy nuclei.

As previously stated, the rotational bands with negative parities of α cluster above doubly magic core have been well reproduced with the "cluster + core" configuration. The assumption of the clustering phenomenon aids comprehension of heavy particle emission and multi-nucleon-transfer reactions [64]. However, the existence of α clusters or heavier clusters in heavy or superheavy nuclei with neutron number $N > 126$ is still an open question owing to the complicated interactions among nucleons and the influence of the mean-field effect. Analogously, analyzing the energy spectra can somewhat confirm the hypothesis of the cluster states in heavy nuclei and further reveal the microscopic mechanisms of nucleon organization and interaction. Consequently, the results of α-cluster structure model shown here serve as a starting point for the next study on exploring the clustering phenomena of heavy nuclei. In the same vein as the strategy in the regular heavy particle emission of superheavy nuclei [65], the doubly magic nucleus ^{208}Pb is still regarded as the frozen core in the framework of BCM. In this sense, the residual component is generalized from an α cluster to the isotopes

TABLE I. Distributions of optimized parameters V_0 in the nuclear potential for heavier cluster states.

Nucleus	Cluster-core	V_0 (MeV)	V_0/A_c (MeV)
^{218}Rn	^{10}Be + ^{208}Pb	360.645 ± 15.904	36.065 ± 1.590
^{220}Rn	^{12}Be + ^{208}Pb	451.804 ± 21.974	37.650 ± 1.831
^{220}Ra	^{12}C + ^{208}Pb	414.750 ± 22.498	34.563 ± 1.875

of Be, C or other heavier clusters. In general, the motion of the wave function, closely related to its energy, provides the rational explanation and description for rotational energy levels. What calls for special attention is the choice of the number n of internal nodes in the radial wave function. Especially for heavy nuclei, the internal nodes n with the previous approach are quite large, even up to 200 which is unreasonable in our framework. In the previous studies [47,61,63], some strategies have been adopted to adjust the n values to describe the parity doublet bands. Considering that the internal nodes n are intimately connected to the depth of the nuclear potential according to our theoretical analysis in Ref. [41], the depth V_0 can be expressed by

$$\frac{V_0}{A_c} = V_1\frac{n^2}{A_c^2} + V_2\frac{n}{A_c} + V_3, \tag{10}$$

where the A_c is the cluster mass number. V_1, V_2, and V_3, the coefficients of the polynomial, are respectively fixed as 6.543 ± 0.996 MeV, −14.443 ± 1.860 MeV, and 31.957 ± 5.888 MeV, which are simultaneously obtained in the following bootstrapping procedure for heavier cluster structures. The depth V_0 for different heavy nuclei can be subsequently determined by Eq. (10). Table I for possible heavier cluster states lists these optimized depths V_0, in which V_0/A_c is not actually identical for different cases. It is to be noted that the experimental information of $K^\pi = 0^-$ negative-parity bands for heavy nuclei is limited. In our studies, the lowest energy bands [55] are selected to try to check the possible cluster-core configuration. With regard to the other parameters in nuclear potential, σ is fixed at 0.342 fm the same as before. After reasonable attempts, a better global description can be achieved through the adjustment of 0.850 fm instead of 0.500 fm for the diffuseness a in heavier-cluster + core configurations of heavy nuclei, which is close to other investigations [35,40,45,47,61]. Thus, the results of residual parameters can be determined as $b = 0.138 \pm 0.059$ and $\lambda = 0.021 \pm 0.009$ fm. It is to be noted that the Gaussian term [45,46] with λ and σ in Eq. (3) compensates the typical shorting of compressed spectra, which comes from the double folding potentials. As expected, the parameter $\lambda = 0.021$ is suitable for reproducing such quite narrow energy bands of negative-parity states as depicted in Refs. [47,61].

Taking these results into consideration, the calculated heavier cluster structures above ^{208}Pb, i.e., ^{12}Be and ^{12}C, are plotted in Fig. 7, in which the lowest rotational bands with negative parities are restricted in a very narrow energy range. The comparison among these results denotes that the theoretical energies of negative-parity states with the cluster + core system describe energy levels well, except for 1^- states

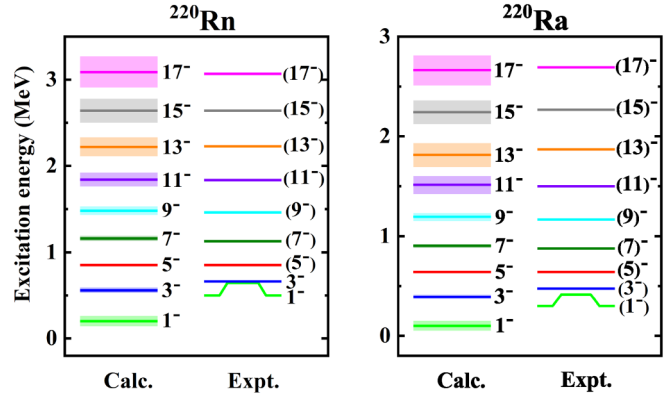

FIG. 7. Comparison of calculated energies with experimental values for the lowest band of negative-parity states in ^{220}Rn (^{12}Be + ^{208}Pb, $G = 63$) and ^{220}Ra (^{12}C + ^{208}Pb, $G = 59$).

as depicted in Fig. 7. The differences of available values [55] between 3^- and 1^- levels are quite small, namely 0.018 MeV for ^{220}Rn and 0.061 MeV for ^{220}Ra. This may mean that the lowest 1^- levels and other lowest levels are not the same energy bands with negative parities. Meanwhile, it is clearly visible that the uncertainty bars have a narrow range. Encouraged by this, the study is directly extended to ^{218}Rn (^{10}Be + ^{208}Pb) to check the integrity of BCM. The energy levels for ^{218}Rn are presented in Fig. 8, which gives excellent reproductions of the complete experimental bands with negative parities. This also clearly indicates that these available levels are possible cluster states for heavy nuclei. A consistent investigation of the negative-parity bands above double shell closures depends on additional experimental data. We hope the present work can provide some theoretical evidence for possible cluster structures in heavy and superheavy nuclei.

IV. CONCLUSION

In summary, the calculations of energy spectra, by combining the binary cluster-core model with the bootstrap method, have been extended to the rotational bands with negative

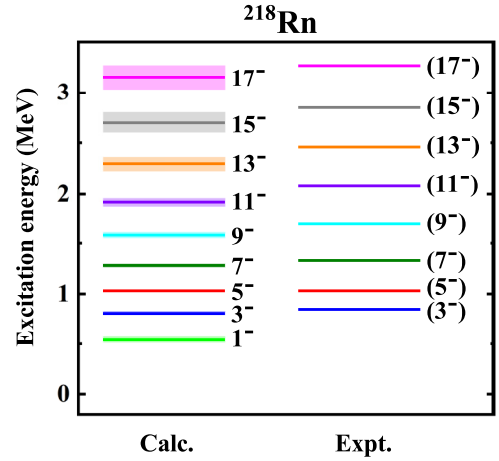

FIG. 8. Same as Fig. 7 but for ^{218}Rn (^{10}Be + ^{208}Pb, $G = 51$).

parities. For ^{20}Ne and ^{44}Ti, the excellent agreement between calculated energy bands and the available data of well-defined α-cluster states demonstrates the applicability of BCM. Furthermore, the energy spectra of selected candidates of cluster states for ^{94}Mo, ^{96}Ru, ^{92}Zr, and ^{98}Pd have been well reproduced in the present framework. The distributions of the model parameter spaces are obtained from multiple resampling, resulting in the calculated levels together with the uncertainty analysis, which can be helpful for ongoing or forthcoming experiments. Encouraged by this, the idea has been extended to the candidates of heavier cluster states with quite narrow energy levels. The corresponding energy spectra are found to be consistent with the observations, plus narrow uncertainty ranges. In general, through the careful statistical analysis of the nonparametric resampling strategy, the BCM is believed to be reliable and stable for interpreting the parity doublet bands from light to heavy nuclei, and is expected to be useful for understanding the cluster degree and clustering phenomenon in the future.

ACKNOWLEDGMENTS

This work is supported by the National Natural Science Foundation of China (Grants No. 12075121 and No. U2267205), by the Natural Science Foundation of Jiangsu Province (Grant No. BK20190067), by the Postgraduate Research & Practice Innovation Program of Jiangsu Province (Grant No. KYCX23_0416), and by the Fundamental Research Funds for the Central Universities (Grant No. 30922010312).

[1] M. Freer, H. Horiuchi, Y. Kanada-En'yo, D. Lee, and U.-G. Meißner, Rev. Mod. Phys. **90**, 035004 (2018).
[2] J. A. Wheeler, Phys. Rev. **52**, 1107 (1937).
[3] G. Gamow, Proc. R. Soc. London A **126**, 632 (1930).
[4] C. Beck, *Clusters in Nuclei: Volume 1*, Lecture Notes in Physics Vol. 818 (Springer, Berlin, 2010).
[5] K. Ikeda, N. Takigawa, and H. Horiuchi, Prog. Theor. Phys. Suppl. **E68**, 464 (1968).
[6] W. von Oertzen, M. Freer, and Y. Kanada-En'yo, Phys. Rep. **432**, 43 (2006).
[7] M. Freer, Rep. Prog. Phys. **70**, 2149 (2007).
[8] J. Chen, Y. Ye, K. Ma, J. Han, D. Wang, C. Lin, H. Jia, L. Yang, G. Li, L. Yang, Z. Hu, Z. Tan, K. Wei, W.-L. Pu, Y. Chen, J. Lou, X. Yang, Q. Li, Z. Yang, T. Luo *et al.*, Sci. Bull. **68**, 1119 (2023).
[9] P. J. Li, D. Beaumel, J. Lee, M. Assié, S. Chen, S. Franchoo, J. Gibelin, F. Hammache, T. Harada, Y. Kanada-En'yo, Y. Kubota, S. Leblond, P. F. Liang, T. Lokotko, M. Lyu, F. M. Marqués, Y. Matsuda, K. Ogata, H. Otsu, E. Rindel *et al.*, Phys. Rev. Lett. **131**, 212501 (2023).
[10] Z. H. Yang, Y. L. Ye, B. Zhou, H. Baba, R. J. Chen, Y. C. Ge, B. S. Hu, H. Hua, D. X. Jiang, M. Kimura *et al.*, Phys. Rev. Lett. **131**, 242501 (2023).
[11] H. Horiuchi, Prog. Theor. Phys. Suppl. **62**, 90 (1977).
[12] S. Pastore, R. B. Wiringa, S. C. Pieper, and R. Schiavilla, Phys. Rev. C **90**, 024321 (2014).
[13] H. Feldmeier, Nucl. Phys. A **515**, 147 (1990).
[14] T. Neff and H. Feldmeier, Nucl. Phys. A **738**, 357 (2004).
[15] Y. Kanada-En'yo, H. Horiuchi, and A. Ono, Phys. Rev. C **52**, 628 (1995).
[16] M. Kimura, T. Suhara, and Y. Kanada-En'yo, Eur. Phys. J. A **52**, 373 (2016).
[17] M. Kimura, Phys. Rev. C **69**, 044319 (2004).
[18] B. Zhou, Y. Funaki, H. Horiuchi, Z. Ren, G. Ropke, P. Schuck, A. Tohsaki, C. Xu, and T. Yamada, Phys. Rev. Lett. **110**, 262501 (2013).
[19] P. Schuck, Y. Funaki, H. Horiuchi, G. Röpke, A. Tohsaki, and T. Yamada, Phys. Scr. **91**, 123001 (2016).
[20] A. Tohsaki, H. Horiuchi, P. Schuck, and G. Röpke, Phys. Rev. Lett. **87**, 192501 (2001).
[21] Y. Funaki, A. Tohsaki, H. Horiuchi, P. Schuck, and G. Röpke, Phys. Rev. C **67**, 051306(R) (2003).
[22] B. Zhou, Y. Funaki, H. Horiuchi, Y. G. Ma, G. Röpke, P. Schuck, A. Tohsaki, and T. Yamada, Nat. Commun. **14**, 8206 (2023).
[23] C. Qi, R. J. Liotta, and R. Wyss, Prog. Part. Nucl. Phys. **105**, 214 (2019).
[24] K. Auranen, D. Seweryniak, M. Albers, A. D. Ayangeakaa, S. Bottoni, M. P. Carpenter, C. J. Chiara, P. Copp, H. M. David, D. T. Doherty, J. Harker, C. R. Hoffman, R. V. F. Janssens, T. L. Khoo, S. A. Kuvin, T. Lauritsen, G. Lotay, A. M. Rogers, J. Sethi, C. Scholey *et al.*, Phys. Rev. Lett. **121**, 182501 (2018).
[25] J. Tanaka, Z. Yang, S. Typel, S. Adachi, S. Bai, P. van Beek, D. Beaumel, Y. Fujikawa, J. Han, S. Heil *et al.*, Science **371**, 260 (2021).
[26] R. G. Lovas, R. J. Liotta, A. Insolia, K. Varga, and D. S. Delion, Phys. Rep. **294**, 265 (1998).
[27] D. S. Delion, R. J. Liotta, and R. Wyss, Phys. Rep. **424**, 113 (2006).
[28] B. Buck, A. C. Merchant, and S. M. Perez, Phys. Rev. Lett. **72**, 1326 (1994).
[29] F. Michel, G. Reidemeister, and S. Ohkubo, Phys. Rev. C **37**, 292 (1988).
[30] B. Buck, A. C. Merchant, and S. M. Perez, Phys. Rev. C **51**, 559 (1995).
[31] T. Yamaya, K. Katori, M. Fujiwara, S. Kato, and S. Ohkubo, Prog. Theor. Phys. Suppl. **132**, 73 (1998).
[32] A. Tohsaki, H. Horiuchi, P. Schuck, and G. Röpke, Rev. Mod. Phys. **89**, 011002 (2017).
[33] S. M. Wang, J. C. Pei, and F. R. Xu, Phys. Rev. C **87**, 014311 (2013).
[34] T. T. Ibrahim, A. C. Merchant, S. M. Perez, and B. Buck, Phys. Rev. C **99**, 064332 (2019).
[35] M. A. Souza and H. Miyake, Phys. Rev. C **91**, 034320 (2015).
[36] H. Horiuchi, K. Ikeda, and K. Kat, Prog. Theor. Phys. Suppl. **192**, 1 (2012).
[37] B. Buck, C. B. Dover, and J. P. Vary, Phys. Rev. C **11**, 1803 (1975).
[38] S. Ohkubo, Phys. Rev. Lett. **74**, 2176 (1995).
[39] F. Michel, G. Reidemeister, and S. Ohkubo, Phys. Rev. C **61**, 041601(R) (2000).
[40] M. A. Souza and H. Miyake, Braz. J. Phys. **35**, 826 (2005).
[41] J. H. Jia, Y. B. Qian, and Z. Z. Ren, Phys. Rev. C **104**, L031301 (2021).

[42] D. Ni and Z. Ren, Phys. Rev. C **83**, 014310 (2011).
[43] D. Bai and Z. Ren, Eur. Phys. J. A **54**, 220 (2018).
[44] M. A. Souza and H. Miyake, Eur. Phys. J. A **59**, 74 (2023).
[45] M. A. Souza, H. Miyake, T. Borello-Lewin, C. A. da Rocha, and C. Frajuca, Phys. Lett. B **793**, 8 (2019).
[46] M. A. Souza and H. Miyake, Phys. Rev. C **104**, 064301 (2021).
[47] B. Buck, A. C. Merchant, and S. M. Perez, Phys. Rev. C **58**, 2049 (1998).
[48] K. Wildermuth and Y. C. Tang, *A Unified Theory of the Nucleus* (Academic Press, New York, 1977).
[49] B. Cai, G. Chen, J. Xu, C. Yuan, C. Qi, and Y. Yao, Phys. Rev. C **101**, 054304 (2020).
[50] Y. Gao, J. Dobaczewski, M. Kortelainen, J. Toivanen, and D. Tarpanov, Phys. Rev. C **87**, 034324 (2013).
[51] C. Yuan, Phys. Rev. C **93**, 034310 (2016).
[52] J. Dobaczewski, W. Nazarewicz, and P. Reinhard, J. Phys. G: Nucl. Part. Phys. **41**, 074001 (2014).
[53] N. Schunck, J. D. McDonnell, D. Higdon, J. Sarich, and S. M. Wild, Eur. Phys. J. A **51**, 169 (2015).
[54] B. Efron, *The Jackknife, the Bootstrap and Other Resampling Plans* (SIAM, Philadelphia, 1982).
[55] http://www.nndc.bnl.gov/ensdf/.
[56] H. Abele and G. Staudt, Phys. Rev. C **47**, 742 (1993).
[57] F. Michel, S. Ohkubo, and G. Reidemeister, Prog. Theor. Phys. Suppl. **132**, 7 (1998).
[58] U. Atzrott, P. Mohr, H. Abele, C. Hillenmayer, and G. Staudt, Phys. Rev. C **53**, 1336 (1996).
[59] T. Yamaya, S. Oh-ami, M. Fujiwara, T. Itahashi, K. Katori, M. Tosaki, S. Kato, S. Hatori, and S. Ohkubo, Phys. Rev. C **42**, 1935 (1990).
[60] R. Storn and K. Price, in *Proceedings of the IEEE International Conference on Evolutionary Computation, Nagoya, 1996* (IEEE, Piscataway, NJ, 1996), pp. 842–844.
[61] T. T. Ibrahim, S. M. Perez, S. M. Wyngaardt, B. Buck, and A. C. Merchant, Phys. Rev. C **85**, 044313 (2012).
[62] P. Mohr, Open Nucl. Part. Phys. J. **1**, 1 (2008).
[63] B. Buck, A. C. Merchant, and S. M. Perez, Phys. Rev. Lett. **76**, 380 (1996).
[64] H. Devaraja, S. Heinz, O. Beliuskina, S. Hofmann, C. Hornung, G. Münzenberg, D. Ackermann, M. Gupta, Y. Gambhir, R. Henderson *et al.*, Eur. Phys. J. A **55**, 25 (2019).
[65] D. N. Poenaru, R. A. Gherghescu, and W. Greiner, Phys. Rev. Lett. **107**, 062503 (2011).